catalysts

MDPI

Article

Investigation of MoO_x/Al_2O_3 under Cyclic Operation for Oxidative and Non-Oxidative Dehydrogenation of Propane

Santhosh K. Matam [1,2], Caitlin Moffat [3], Pip Hellier [1,2], Michael Bowker [1,2], Ian P. Silverwood [1,4], C. Richard A. Catlow [1,2,5], S. David Jackson [3], James Craswell [1,6], Peter P. Wells [1,6,7], Stewart F. Parker [1,3,4] and Emma K. Gibson [1,3,*]

1 UK Catalysis Hub, Research Complex at Harwell, STFC Rutherford Appleton Laboratory, Harwell OX11 0FA, UK; santhosh.matam@rc-harwell.ac.uk (S.K.M.); pip.hellier@rc-harwell.ac.uk (P.H.); BowkerM@cardiff.ac.uk (M.B.); ian.silverwood@stfc.ac.uk (I.P.S.); CatlowR@cardiff.ac.uk (C.R.A.C.); jac1g14@soton.ac.uk (J.C.); ppwells@soton.ac.uk (P.P.W.); stewart.parker@stfc.ac.uk (S.F.P.)
2 Cardiff Catalysis Institute, School of Chemistry, Cardiff University, Park Place, Cardiff CF10 1AT, UK
3 School of Chemistry, Joseph Black Building, University of Glasgow, Glasgow G12 8QQ, UK; c.moffat.1@research.gla.ac.uk (C.M.); David.Jackson@glasgow.ac.uk (S.D.J.)
4 ISIS Neutron and Muon Source, STFC Rutherford Appleton Laboratory, Oxon OX11 0QX, UK
5 Department of Chemistry, University College London, 20 Gordon St, London WC1 HOAJ, UK
6 School of Chemistry, University of Southampton, University Road, Southampton SO17 1BJ, UK
7 Diamond Light Source, Harwell Science and Innovation Campus, Chilton, Didcot OX11 0DE, UK
* Correspondence: Emma.Gibson@glasgow.ac.uk

Received: 28 October 2020; Accepted: 22 November 2020; Published: 24 November 2020

Abstract: A MoO_x/Al_2O_3 catalyst was synthesised and tested for oxidative (ODP) and non-oxidative (DP) dehydrogenation of propane in a reaction cycle of ODP followed by DP and a second ODP run. Characterisation results show that the fresh catalyst contains highly dispersed Mo oxide species in the +6 oxidation state with tetrahedral coordination as $[Mo^{VI}O_4]^{2-}$ moieties. In situ X-ray Absorption Spectroscopy (XAS) shows that $[Mo^{VI}O_4]^{2-}$ is present during the first ODP run of the reaction cycle and is reduced to $Mo^{IV}O_2$ in the following DP run. The reduced species are partly re-oxidised in the subsequent second ODP run of the reaction cycle. The partly re-oxidised species exhibit oxidation and coordination states that are lower than 6 but higher than 4 and are referred to as Mo_xO_y. These species significantly improved propene formation (relatively 27% higher) in the second ODP run at similar propane conversion activity. Accordingly, the initial tetrahedral $[Mo^{VI}O_4]^{2-}$ present during the first ODP run of the reaction cycle is active for propane conversion; however, it is unselective for propene. The reduced $Mo^{IV}O_2$ species are relatively less active and selective for DP. It is suggested that the Mo_xO_y species generated by the reaction cycle are active and selective for ODP. The vibrational spectroscopic data indicate that the retained surface species are amorphous carbon deposits with a higher proportion of aromatic/olefinic like species.

Keywords: propane; dehydrogenation; molybdenum oxide; XANES; Raman spectroscopy; inelastic neutron scattering spectroscopy; infrared spectroscopy

1. Introduction

In order to bridge the propene supply and demand gap, the chemical industry has looked to highly selective on-purpose technologies like propane dehydrogenation (DP). Despite the selectivity benefits of DP, the process is highly endothermic and vulnerable to fast catalyst deactivation. Alternatively, propane oxidative dehydrogenation (ODP) occurs in the presence of oxygen via an exothermic pathway

which has the potential to overcome the thermodynamic and catalyst deactivation constraints inherent in DP. The commercialisation of ODP is however not yet feasible, due to propene selectivities being hampered by consecutive combustion reactions [1–5].

In order to overcome this problem, studies have been conducted into the use of supported molybdenum oxide to enhance selectivity for propylene during ODP and DP reactions [3,5,6]. Molybdenum oxide-based catalysts have been well characterised by various techniques including operando methods due to their fundamental and applied significance [7–14]. It is widely accepted that the nature and distribution of Mo oxide species depend sensitively on several parameters such as Mo loading, catalyst support and calcination procedure, resulting in a variety of species spanning from monomeric, dimeric and oligomeric Mo oxide species to large Mo oxide clusters [8,11,15–17]. The surface composition of the catalyst determines the catalytic properties in various petro- and fine- chemical processes such as oxidation, metathesis, aromatisation and dehydrogenation of lower alkanes [15,18–24]. For example, by in situ Raman studies on MoO_x/Al_2O_3 it is suggested that oligomeric Mo oxide species are more active for propene metathesis than monomeric species or large clusters [15], while oxidative dehydrogenation of ethane (ODE) activity is related to monomeric Mo–O–Al species [17]. Other studies on MoO_x/ZrO_2 suggest that Mo=O species are active for C–H bond activation in oxidative dehydrogenation of propane (ODP) [16]. In a marked contrast, another study on MoO_x/Al_2O_3 promoted with Li suggests that terminal Mo=O species are not active for ODP [25].

Chemical-looping strategies have also been recently explored for DP in order to combat the undesired combustion reactions and subsequently improve propylene selectivity [26,27]. Propene selectivity was studied over 10 propane only injections (no O_2 in the feed) followed by a re-oxidation step over vanadium catalysts. Combustion to carbon oxides dominated during the first few injections, followed by an increasing propene selectivity, implying that a degree of catalyst reduction is necessary to maximise propene selectivity [26]. Similar DP studies over mixed Mo-V-O catalysts have reported 100 cycles of PD followed by regeneration, yielding promising propene yields [27]. An operando UV-Vis/Raman/XAFS study on MoO_x/Al_2O_3 during successive propane dehydrogenation (DP) cycles consisting of reaction and regeneration indicates reduction of some of the initial Mo^{VI} to Mo^{IV} and changes in the catalyst structure along with coke formation which accounted for a continuous loss in overall activity in successive cycles [28].

In line with these observations, the present study reports a novel reaction cycle comprising ODP, DP followed by a second ODP run over MoO_x/Al_2O_3. Significantly, the reaction cycle results in increased propene formation in the second ODP reaction whilst maintaining a similar propane conversion. The improved propene formation is explained by in situ X-ray Absorption Near Edge Structure (XANES) and the nature of surface adsorbed species under the reaction cycle is probed by complementary Raman, infrared and inelastic neutron scattering (INS) spectroscopy studies.

2. Results and Discussion

2.1. Activity Tests

The catalyst activity in sequential oxidative (ODP) and non-oxidative (DP) dehydrogenation of propane cycle is presented in Figure 1. On switching to the first ODP step an initial propane conversion of ~30% was observed which gradually dropped to 25.5% after 30 min on stream. After a subsequent regeneration step, a slight increase in conversion was observed at the onset of propane dehydrogenation (26.5%) however, this dropped continually over the 60 min reaction period. On switching back to ODP, a gradual recovery of the catalyst activity was observed, reaching 26.5% after ~35 min. This gain of 24.5% was identical to the lost activity observed during the previous DP run. The regained activity can be attributed to the combustion of the surface adsorbed species (a sharp CO_2 and H_2O formation appeared at the initial stage of the second ODP, not shown) which perhaps recovers a fraction of the active Mo oxide sites. At the end of the second ODP reaction cycle, the activity of the catalyst is similar

to the one observed at the end of the first ODP run indicating that deactivation observed during the 60 min DP was reversible.

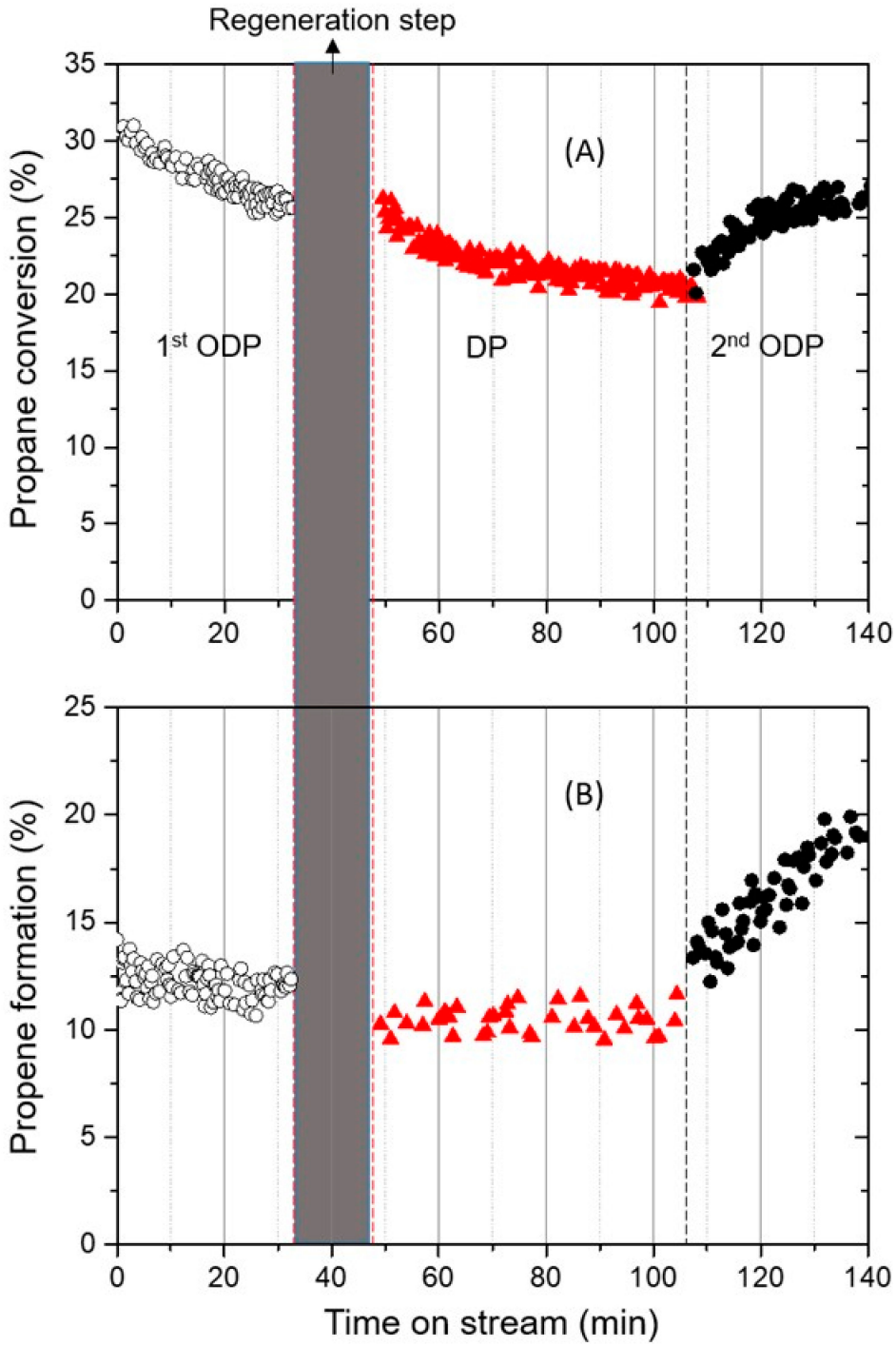

Figure 1. The subsequent oxidative and non-oxidative dehydrogenation of propane activity over MoO_x/Al_2O_3 at 500 °C shown as (**A**) Propane conversion and (**B**) Propene formation. Propene formation is presented as the contribution of propene to the mass spectrometry response of m/z 41 expressed as a%. This is calculated by subtracting the contribution of propane to m/z 41. Refer to the Materials and Methods section for activity test details.

Interestingly, the propene selectivity got markedly better during the second ODP reaction, increasing from a contribution to m/z 41 of 10% during the DP cycle, to almost 20% by the end of the

second ODP cycle (Figure 1B). Significantly, the propene formation was substantially improved (5%) in the second ODP run as compared to that in the first ODP at similar propane conversion. Within the first 10 min on stream of the second ODP run, the oxygen content in the feed considerably depleted suggesting the combustion of carbon deposits and perhaps occurrence of a Mo oxide redox cycle. The former is consistent with the rapid formation of CO_2 and H_2O as noted above. Excluding these first 10 min of the second ODP run which can be attributed to coke combustion, the amount of CO_2 formed in both ODP runs was approximately equal, no CO_2 is detected under DP. Despite significant differences in propene formation in the first and second ODP runs, similar CO_2 formation indicated the occurrence of competitive reactions (other than combustion) such as aromatization, which is known for Mo oxide based catalysts [11,15,18–21]. Such side reactions might have dominated in the first ODP run while they appeared to have been suppressed in the second ODP. The improved propene formation and suppressed side reactions in the second ODP may have been a result of the DP run that fell between the two ODP runs of the reaction cycle. Therefore, the effect of reaction cycle on the nature of active/selective Mo oxide species and the nature of surface adsorbed species is of interest. To this end, in situ XANES, which is sensitive to the oxidation and coordination state of Mo oxide, under the reaction cycle was studied to capture the redox dynamics of the catalyst.

2.2. In-Situ XANES

The in situ XANES experiment replicates the reaction cycle and was used to monitor Mo oxide species. The XANES spectrum of the fresh catalyst, Figure 2A resembles the spectrum of the reference compound $Fe_2(MoO_4)_3$, with an edge (E_0) energy of 20017.3 eV and a similar intense pre-edge feature due to an $s \rightarrow d$ electronic transition, suggesting that the oxidation and coordination states of the Mo oxide species in the fresh catalyst were similar to the reference compound $Fe_2(MoO_4)_3$. Such an electronic transition from $s \rightarrow d$ is Laporte forbidden, however, a significant p-d hybridization of a system with a tetrahedral geometry that is highly distorted may allow the transition due to a net change in the parity ($\Delta l = 1$) [29]. Based on this, it can be proposed that Mo oxide species in the fresh catalyst were in the +6 oxidation state (Table 1) with tetrahedral coordination as in $[Mo^{VI}O_4]^{2-}$ [29,30].

After the first ODP run of the reaction cycle, no changes to the XANES spectra were observed as compared to that of the fresh catalyst (Figure 2), implying no change in the oxidation and coordination state of $[Mo^{VI}O_4]^{2-}$ species. The following 60 min DP run resulted in a gradual change in the pre-edge and edge features. At the end of this period, the sharp pre-edge feature was diminished and edge features became distinctly prominent, consistent with a change in the coordination state of $[Mo^{VI}O_4]^{2-}$ from tetrahedral to more octahedral-like in character that forbade the $s \rightarrow d$ transition. [29,31] The edge position also shifted gradually from 20017.3 eV to 2014.4 eV as shown in Figure 2B, the latter coinciding with that of reference MoO_2 indicating that the oxidation state of $[Mo^{VI}O_4]^{2-}$ species in the catalyst was reduced from +6 to +4 (Figure 2A). During the first 10 min of the second ODP run the edge position of the XANES spectrum shifted steadily from 2014.4 eV to 20,016.9 eV, after which no further change was observed. Interestingly, the edge position at 20,016.9 eV was lower than the one observed for the fresh catalyst and that after the first ODP run but was higher than the edge position observed after the intermediate DP run, indicating that only partial re-oxidation of Mo oxide occurred during the second ODP run, coinciding with the depleted oxygen content in the feed during the reaction cycle (see Activity Tests section). Thus, the edge position of the spectrum taken at the end of the second ODP run, which was also the end of the reaction cycle, fell between the Mo oxidation state of +6 and +4. Moreover, the altered intensity of the pre-edge feature implies that the tetrahedral $[Mo^{VI}O_4]^{2-}$ species were not completely recovered. These observations indicate that at the end of the reaction cycle a fraction of Mo oxide species appeared to be in a distorted structure, which was neither fully octahedral nor tetrahedral with an oxidation state lower than +6 but higher than +4, formed at the expense of the initial tetrahedral $[Mo^{VI}O_4]^{2-}$ species.

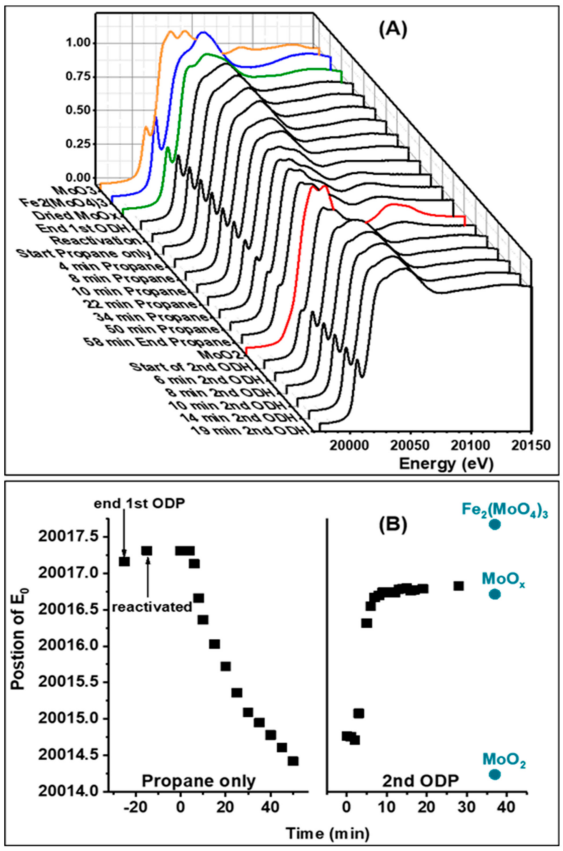

Figure 2. In situ X-ray Absorption Near Edge Structure (XANES) spectra of MoO_x/Al_2O_3 at 500 °C during oxidative and non-oxidative dehydrogenation of propane cycle (**A**) and the change in the position of the edge energy of the XANES during on stream of the reaction cycle (**B**). XANES spectra and edge energies of the reference compounds MoO_3, $Fe_2(MoO_4)_3$ and MoO_2 are also included.

Analysis of the Extended X-ray Absorption Fine Structure (EXAFS) region of the spectra collected at the end of the first ODH run was consistent with $[MoO_4]^{2-}$ species, fitting well to 4 M-O scatterers with a distance of 1.74 Å. After the DP run, the catalyst appeared to be reduced, fitting to two Mo-O paths at distances similar to MoO_2 [30]. In comparison to the first ODP run, at the end of the second ODP run, the data required a second Mo-O scattering path at 1.9 Å, indicating a greater spread in O distances consistent with MoO_x species retaining some of the octahedral character obtained during the DP run (Table 1). The reaction cycle induced rearrangement of Mo oxide species in the catalyst was further studied by Raman spectroscopy.

Table 1. Extended X-ray Absorption Fine Structure (EXAFS) fitting parameters [1] for the spectra collected at the end of step of the reaction cycle.

Sample	Abs-Scatterer	E_0 (eV)	Coordination Number	R (Å)	σ^2	R_{factor}
End of 1st ODP	Mo-O	−8.0 ± 0.3	4 ± 1	1.74 ± 0.01	0.006 ± 0.004	0.05
End of DP	Mo-O Mo-O	5 ± 8	1.0 ± 0.7 2.8 ± 0.8	1.76 ± 0.03 2.06 ± 0.04	0.003 0.003	0.1
End of 2nd ODP	Mo-O Mo-O	−9 ± 7	4.2 ± 0.6 1.3 ± 0.9	1.74 ± 0.04 1.96 ± 0.07	0.005 0.003	0.04

[1] Fitting parameters: S_0^2 determined from the Mo foil = 0.82, 1 < R < 3 Å, k-range 3.0–10.0 $Å^{-1}$, no. of independent points 9.

2.3. Raman Spectra

The Raman spectrum of the fresh catalyst (before the reaction cycle) showed bands at 374, 814, 884, 920 and 1000 cm^{-1} with shoulders at 993 and 1025 cm^{-1}, Figure 3 and detailed in Table 2. The spectrum largely resembles the reference compounds $Al_2(MoO_4)_3$ and $Fe_2(MoO_4)_3$ [11] indicating the presence of at least three types of highly distorted MoO_4 like species in the fresh catalyst, in excellent agreement with the XANES data that showed a pre-edge $s \rightarrow d$ electron transition indicating a distorted tetrahedral geometry. The band at 815 cm^{-1} may indicate the presence of a small amount of MoO_3, however, the accompanying bands expected between 700 and 500 cm^{-1} attributable to Mo–O–Mo bonds in polycrystalline MoO_3 particles [7–9,11,15,16] were not observed, which suggests the majority of the Mo was isolated $[MoO_4]^{2-}$ species. The presence of highly dispersed oligomeric/polymeric species cannot be ruled out as the corresponding bands were probably overlapped by bands between 376 and 800–1000 cm^{-1} [11,15].

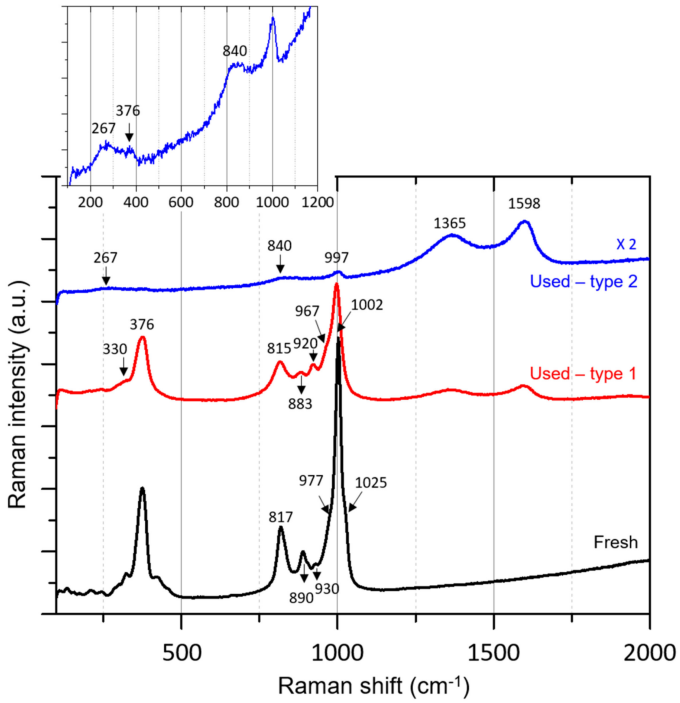

Figure 3. Raman spectra of hydrated fresh (before the reaction) and used (after the reaction cycle) catalysts at room temperature. Magnified region of the used catalyst—type 2 is shown in the inset.

Table 2. Proposed assignments [1] of observed Raman bands.

Sample	Wavenumber (cm^{-1})	Mode [2]	Mo Species
Fresh	1025	ν(Mo=O)	$Al_2(MoO_4)_3$
	1000	ν(Mo=O)	$Al_2(MoO_4)_3$ or MoO_3
	993	ν(Mo–O)	$Al_2(MoO_4)_3$ or MoO_3
Used Type 1	965	ν(Mo–O)	Octahedral Mo species
	930	ν_s(Mo–O)	Dimeric
Fresh + Used Type 1	884	ν_{as}(Mo–O)	Dimeric
Used Type 2	840	ν(Mo–O–Mo) or ν(Mo–O–Al)	Mo^{5+}
Fresh + Used Type 1	814	ν_{as}(Mo–O–Mo)	MoO_3
Fresh + Used Type 1 + 2	374	δ(Mo=O)	$Al_2(MoO_4)_3$
Used Type 2	267	δ(Mo–O–Mo)	Polymerized species

[1] Assignments of the Raman data are taken from references 7, 11, 20, 31 and 32. [2] Modes are described where ν and δ represent stretch and bend respectively, and as and s represent asymmetric and symmetric.

After the reaction cycle (used catalyst), two distinct Raman spectra were noted indicating that the catalyst bed was unevenly affected, as expected, from the inlet to the outlet region (Figure 3). The type-1 Raman spectrum (red spectrum in Figure 3) of the catalyst resembled that of the fresh catalyst, however, the absolute intensity was reduced and the position of the bands was slightly red shifted. Moreover, two weak additional bands at 1365 and 1598 cm^{-1} were present. The band positions were now centred at 815, 883, 920 and 997 with a shoulder at 965 cm^{-1}. We note that the high frequency shoulder observed for the fresh catalyst at 1025 cm^{-1} was missing and the band at 376 cm^{-1} became broader with an extended tail in the low energy region. These observations indicate a decreased population of mono oxo tetrahedral Mo species in favour of polymeric species, including octahedral (965 and 920 cm^{-1}) and dimeric species (930, 883, and 330 cm^{-1}), but not in favour of polycrystalline MoO_3 particles as is evident from the missing bands between 700 and 500 cm^{-1}. In line with this, the type-2 Raman spectrum (blue) showed weak and broad bands assignable to Mo oxide species at 267, 376, 840 and 1000 cm^{-1} (see inset in Figure 3), along with two additional prominent bands at 1365 and 1598 cm^{-1}. The band at 267 cm^{-1} could be tentatively attributed to the Mo–O–Mo bond in polymerized species, while the band at 840 cm^{-1} could be assigned to terminal Mo=O bonds [32] or to reduced Mo oxide species with an oxidation state of +5 [20,33]. The latter was in excellent agreement with in situ XANES results which showed an oxidation state of $4 < \delta < 6$ (Figure 2 and Table 2) and indicated the changed nature and distribution of Mo oxide species in the catalyst. The two distinct Raman spectra of the used catalyst exhibit common bands at 1365 cm^{-1} and 1598 cm^{-1} which are attributable to carbon deposits [34]. The band at 1365 cm^{-1} is denoted as the D band, also referred to as the disorder-induced mode, and relates to the A_{1g} mode [34,35]. The band at 1598 cm^{-1} was denoted as the G band and related to the E_{2g} mode [35]. Among the two, the G band was sharper and more intense than the D band implying the graphitic-like structure of the adsorbed species which was further studied by infrared spectroscopy.

2.4. Diffuse Reflectance Infrared Fourier Transform Spectroscopy (DRIFTS)

The DRIFTS spectra of the fresh and used catalysts are shown in Figure 4. The fresh catalyst showed broad bands centred around 3500, 3250, 1624, 1420 and 1060 cm^{-1}. The bands at 3500 and 3250 cm^{-1} were assigned to the stretching modes of hydrogen bonded OH groups on the catalyst surface (including physisorbed water) [36–38]. The corresponding H–O–H bending mode appeared at 1624 cm^{-1}. The bands at 1420 and 1060 cm^{-1} could be due to surface adsorbed carbonate-like species and surface Al–O vibrational mode of the support γ-Al_2O_3, respectively [39,40]. The broad features between 1060 and 800 cm^{-1} were tentatively assigned to isolated $[Mo^{VI}O_4]^{2-}$ like species [20,40,41], in line with the in situ XANES and Raman spectra (Figures 2 and 3).

The used catalyst exhibited several new bands below 2000 cm^{-1} (Figure 4). The bands at 1690, 1585, 1420, 1367, 1165 and 1025 cm^{-1} reflected the surface adsorbed species resulting from the reaction cycle. These bands may very well represent different species which overlap at the same position. The weak band at 1690 cm^{-1} may be the C=C stretch mode of substituted alkenes [42,43], or it may reflect the presence of a small amount of a conjugated ketonic functionality. The prominent band at 1585 cm^{-1} was assigned to aromatic C=C stretching modes. In line with this, the band at 1024 cm^{-1} could also be due to aromatic C–H deformation mode [42,44]. The band at 1420 and a broad feature at 1367 cm^{-1} could be due to in plane $\delta(=CH_2)$ and $\delta_{sym}CH_3$ modes of alkenes [42,44]. The corresponding C–C stretching and methyl rock modes of alkenes may have contributed to bands at 1165 and 1024 cm^{-1}, respectively. A contribution from surface carbonate species to bands at 1580 and 1420 cm^{-1} [39,45] was unlikely under these reaction conditions. The results on the one hand indicated the presence of complex combination of surface adsorbed species which were olefinic and aromatic in nature on the used catalyst, on the other hand reflected the complexity of IR bands which required additional evidence such as by inelastic neutron scattering (INS).

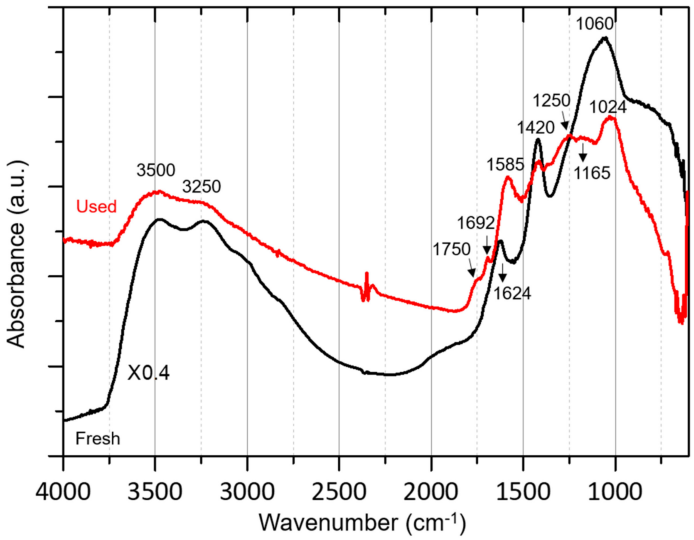

Figure 4. Diffuse Reflectance Infrared Fourier Transform (DRIFT) spectra of fresh (before the reaction) and used (after the reaction) hydrated catalysts at room temperature.

2.5. Inelastic Neutron Scattering (INS) Spectroscopy

INS is a complementary technique to the traditional infrared and Raman spectroscopy and is sensitive to the hydrogenous species of the surface adsorbed deposits [46]. Thus, the catalyst before and after the reaction cycle is studied by INS to shed more light on the structure of the adsorbed species, Figure 5.

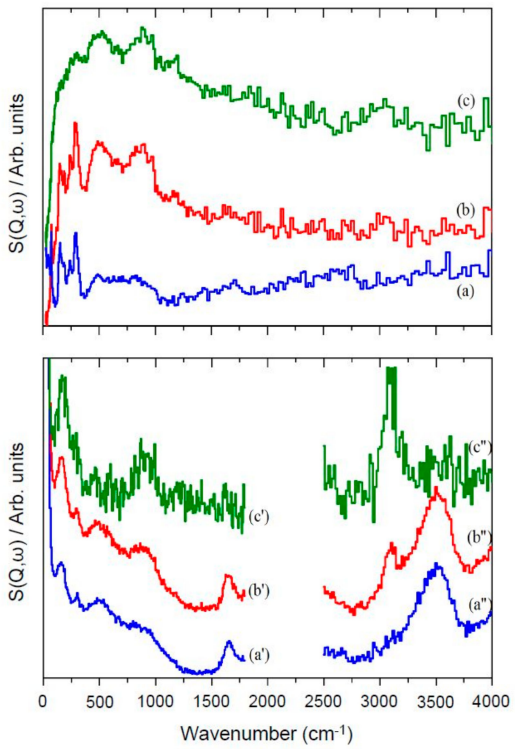

Figure 5. Inelastic Neutron Scattering (INS) spectra of: (a) fresh (before the reaction), (b) used (after the reaction cycle) catalysts and (c) the difference spectra. The top set was recorded on TOSCA, with the fresh catalyst recorded immediately after drying in vacuum at 110 °C. The lower set were recorded with MAPS using incident energies of 2000 cm^{-1} (a′, b′, c) and 5200 cm^{-1} (a″, b″, c″). The fresh catalyst

used for the MAPS measurements (a′ and a″) was the same as that used for TOSCA (a), however, the measurement delay between the two beam times (TOSCA and MAPS) led to water re-absorption on the catalysts.

The difference spectrum in the TOSCA data ((c) in the top part of Figure 5) showed a broad feature at ~500 cm^{-1}, a second feature at ~900 cm^{-1} and a very weak mode at ~3100 cm^{-1}. In the corresponding difference spectrum of the MAPS data (lower part of Figure 5), the 900 and 3100 cm^{-1} features were also seen, but not the ~500 cm^{-1} one. The band at 500 cm^{-1} observed on the used catalysts is due to the librational modes of adsorbed water. As the fresh catalyst had been dried under vacuum just prior to measurement, this mode was not observed for the fresh sample and therefore is not subtracted in the resulting spectrum. As both the fresh and used catalysts used for the MAPS measurements were partially re-hydrated, the water bands were well subtracted, as shown in the MAPS difference spectra. The two bands at 900 and 3100 cm^{-1} were assigned as the out-of-plane C–H bend and the C–H stretch of a furnace black-like species [47,48], while the weak band at ~1230 cm^{-1} is due to an in-plane C–H bend. Based on this, it can be suggested that the surface carbonaceous deposits were mainly aromatic-like species with furnace black-like structure. Previous work using GC-MS identified pyrene, methyl pyrene and perylene species [49], these are likely to be precursors to the material observed by INS spectroscopy. However, the occurrence of a fraction of olefinic coke-like species cannot be ruled out as shown by the DRIFTS.

3. Materials and Methods

3.1. Catalyst Synthesis

The Mo oxide supported on γ-Al_2O_3 catalyst was prepared by the incipient wetness impregnation method. A clear colourless aqueous solution of ammonium molybdate tetrahydrate (99%, Fluka analytical, Loughborough, UK) was added dropwise to γ-Al_2O_3 (Degussa, AG, Düsseldorf, Germany), which was previously calcined at 500 °C for 5 h. The impregnated sample was then dried at 120 °C for 12 h, followed by calcination at 500 °C for 24 h, which resulted in a pale-yellow powder. This consisted of, nominally, three monolayers (≈21 wt.%) Mo oxide on Al_2O_3 support (Table 3). The final calcined catalyst was denoted as fresh catalyst MoO_x/Al_2O_3.

Table 3. Physico-chemical properties of the catalysts.

Catalyst	V_{total} (cm^3/g)	S_{BET} [a] (m^2/g)	Pore Size [b] (nm)	Surface Mo Density (Mo/nm^2) [c]	Oxidation State of Mo Oxide [d]
Fresh	0.612	81	16	10.8	VI
Used	0.610	79.0	16	11.1	IV < δ < VI

[a] Brunauer–Emmett–Teller (BET) method; [b] Barrett-Joyner-Halenda (BJH) model; [c] nominal loading; [d] XANES.

3.2. Activity Tests

The catalyst activity and selectivity in a subsequent oxidative (ODP) and non-oxidative (DP) dehydrogenation of propane cycle were studied at 500 °C using a commercial Hiden Analytical micro reactor (CATLAB, Warrington, England). The reactor inlet was connected to a gas manifold and the outlet was connected to a Hiden Analytical QGA mass spectrometer, Warrington, England. The reactor was loaded with 50 mg of catalyst (sieve fraction ≈150 μm). Prior to the reaction cycle, the catalyst was pre-treated in air at 500 °C for 30 min. Then the air was replaced by the reaction mixture (at a total flow of 50 mL min^{-1}) corresponding to the subsequent ODP and DP reaction cycle which comprises of: 4 vol.% C_3H_8 and 2 vol.% O_2 in He (first ODP run for 30 min), followed by 10 vol.% O_2 in He (a regeneration step for 15 min) and then 5 vol.% C_3H_8 in He (DP run for 60 min) and finally the second ODP run with the same mixture as for the first ODP run for 30 min. Propene formation is presented as the contribution of propene to the mass spectrometry response of m/z 41 expressed as a%. This was calculated by subtracting the contribution of propane to m/z 41.

3.3. In Situ X-ray Absorption Near Edge Structure (XANES)

In situ XANES measurements were conducted on the B18 beamline at the Diamond Light Source (Harwell, UK). Measurements were performed in transmission using a QEXAFS setup with fast scanning Si(311) monochromator at the Mo K edge. A Harrick X-ray transmission DRIFTS cell mounted on to a Da Vinci arm, was used for the reactions, fitted with glassy carbon windows for X-ray transmission and ZnSe windows for DRFITS measurements, details of the setup are reported elsewhere [50]. The XANES spectra were collected with a time resolution of 60 s/spectrum. Ion chamber detectors were used to determine intensities of the incident (I0) and transmitted (It) X-rays. In situ XANES spectra were collected at 500 °C during the reaction cycle (ODP-DP-ODP), using the same reaction protocol and mixture as noted above. The XANES data was processed using the IFEFFIT with the with the Horae package (Athena and Artemis, Demeter 0.9.25, IFEFFIT 1.2.12) [51,52]. DRIFTS spectra were simultaneously recorded, using an Agilent Carey 680 spectrometer with MCT detector, but due to a faulty detector these data were repeated offline.

3.4. Characterization

Nitrogen absorption and desorption isotherms were collected at −196 °C on a Quantachrome QUADRASORB evo instrument (model QDS-30), (Boynton Beach, FL, USA). The catalysts were degassed at 150 °C for 12 h (using a Quantachrome FLOVAC Degasser equipment) and then the total surface area of the catalysts was measured by the Brunauer–Emmett–Teller (BET) method.

Raman spectra were collected with 514 nm excitation using a Renishaw microscope. The spectra were recorded with an acquisition time of 10 s for six accumulations.

DRIFTS experiments were performed using an Agilent Cary 680 FTIR series spectrometer, (Agilent Technologies, Wokingham, UK) equipped with a Harrick Praying Mantis reaction cell. Spectra were recorded by taking 64 scans with a resolution of 4 cm^{-1} using a liquid nitrogen cooled MCT detector.

INS spectra were collected using TOSCA and MAPS spectrometers [46] at the ISIS Neutron and Muon Source. A large quantity (5–10 g) of catalyst is generally required to obtain an INS spectrum with a reasonable signal-to-noise ratio. Thus, the sample was prepared separately using a laboratory scale fixed bed reactor with similar reaction conditions that were used for activity tests on the micro-reactor (see Activity test section). Small aliquots of these samples were used for the Raman and DRIFTS measurements. The used catalysts, ≈8 g, were wrapped in aluminium foil and then loaded into thin walled aluminium cans for INS measurements. The two spectrometers were complementary: TOSCA provided high quality spectra in the 0–2000 cm^{-1} range, while MAPS enabled the C–H and O–H stretch region to be measured.

4. Conclusions

A novel reaction cycle consisting of oxidative (ODP) and non-oxidative (DP) dehydrogenation of propane followed by the second ODP is tested over MoO_x/Al_2O_3. In situ XANES shows that the reaction cycle leads to formation of active and selective Mo_xO_y species for ODP as evident from the increased propene formation which is 27% relatively higher in the second ODP run. Crucially, the increased propene formation is achieved at a similar propane conversion of around 25%. The active and selective Mo_xO_y species are in a distorted structure with oxidation and coordination states lower than 6 but higher than 4 and are formed at the expense of the initial tetrahedral $[Mo^{VI}O_4]^{2-}$ moieties which are present in the fresh catalyst (i.e., before the reaction cycle). The initial $[Mo^{VI}O_4]^{2-}$ moieties of the fresh catalyst are active for propane conversion but unselective for propene. In situ XANES also show that during the DP run the $[Mo^{VI}O_4]^{2-}$ species are reduced to $Mo^{IV}O_2$ which are relatively less active for propane conversion and less selective for propene. The resulting surface adsorbed species accumulated on the catalyst at the end of the reaction cycle, after the catalyst activity was restored and propene selectivity observed to improve, are in general, amorphous carbon deposits with a furnace black-like structure and has interesting implications for the catalyst durability.

Author Contributions: The authors have contributed in the following ways: conceptualization, E.K.G., S.F.P., C.R.A.C. and M.B.; methodology, I.P.S., P.P.W., S.F.P.; E.K.G., validation, S.D.J.; formal analysis, S.K.M., E.K.G., S.F.P., P.P.W.; investigation, S.K.M., J.C., E.K.G., C.M., P.H., P.P.W.; writing—original draft preparation, S.K.M., C.M.; writing—review and editing, S.F.P. and E.K.G.; supervision, E.K.G., S.K.M., S.D.J.; funding acquisition, C.R.A.C., E.K.G. All authors have read and agreed to the published version of the manuscript.

Funding: This research was funded by the Engineering and Physical Sciences Research Council (EPSRC) through grants: EP/I038748/1, EP/I019693/1, EP/K014706/1, EP/K014668/1, EP/K014854/1, EP/K014714/1 and EP/M013219/1.

Acknowledgments: The UK Catalysis Hub is thanked for resources and support provided via membership of the UK Catalysis Hub Consortium. We thank the Diamond Light Source for provision of beam time (SP10306) on B18. The STFC Rutherford Appleton Laboratory is thanked for access to neutron beam facilities [53,54].

Conflicts of Interest: The authors declare no conflict of interest.

References

1. Kung, H.H. Oxidative dehydrogenation of light (C_2 to C_4) alkanes. *Adv. Catal.* **1995**, *40*, 1–38. [CrossRef]
2. Cavani, F.; Trifirò, F. The oxidative dehydrogenation of ethane and propane as an alternative way for the production of light olefins. *Catal. Today* **1995**, *24*, 307–313. [CrossRef]
3. Mamedov, E.A.; Cortés-Corberan, V. Oxidative dehydrogenation of lower alkanes on vanadium oxide-based catalysts. The present state of the art and outlooks. *Appl. Catal. A* **1995**, *127*, 1–40. [CrossRef]
4. Wachs, I.E.; Weckhuysen, B.M. Structure and reactivity of surface vanadium oxide species on oxide supports. *Appl. Catal. A* **1997**, *157*, 67–90. [CrossRef]
5. Blasco, T.; López-Nieto, J.M. Oxidative dyhydrogenation of short chain alkanes on supported vanadium oxide catalysts. *Appl. Catal. A* **1997**, *157*, 117–142. [CrossRef]
6. Bañares, M.A. Supported metal oxide and other catalysts for ethane conversion: A review. *Catal. Today* **1999**, *51*, 319–348. [CrossRef]
7. Wachs, I.E. Raman and IR studies of surface metal oxide species on oxide supports: Supported metal oxide catalysts. *Catal. Today* **1996**, *27*, 437–455. [CrossRef]
8. Radhakrishnan, R.; Reed, C.; Oyama, S.T.; Seman, M.; Kondo, J.N.; Domen, K.; Ohminami, Y.; Asakura, K. Variability in the structure of supported MoO_3 Catalysts: Studies using Raman and x-ray absorption spectroscopy with ab initio calculations. *J. Phys. Chem. B* **2001**, *105*, 8519–8530. [CrossRef]
9. Bañares, M.A.; Wachs, I.E. Molecular structures of supported metal oxide catalysts under different environments. *J. Raman Spectrosc.* **2002**, *33*, 359–380. [CrossRef]
10. Briand, L.E.; Tkachenko, O.P.; Guraya, M.; Wachs, I.E.; Grünert, W. Methodical aspects in the surface analysis of supported molybdena catalysts. *Surf. Interface Anal.* **2004**, *36*, 238–245. [CrossRef]
11. Tian, H.; Roberts, C.A.; Wachs, I.E. Molecular structural determination of molybdena in different environments: Aqueous solutions, bulk mixed oxides, and supported MoO_3 catalysts. *J. Phys. Chem. C* **2010**, *114*, 14110–14120. [CrossRef]
12. Bergwerff, J.A.; Visser, T.; Leliveld, B.R.G.; Rossenaar, B.D.; de Jong, K.P.; Weckhuysen, B.M. Envisaging the physicochemical processes during the preparation of supported catalysts: Raman microscopy on the impregnation of Mo onto Al_2O_3 extrudates. *J. Am. Chem. Soc.* **2004**, *126*, 14548–14556. [CrossRef]
13. Bentrup, U.; Radnik, J.; Armbruster, U.; Martin, A.; Leiterer, J.; Emmerling, F.; Brückner, A. Linking simultaneous in situ WAXS/SAXS/Raman with Raman/ATR/UV–vis Spectroscopy: Comprehensive insight into the synthesis of molybdate catalyst precursors. *Top. Catal.* **2009**, *52*, 1350–1359. [CrossRef]
14. Gibson, E.K.; Zandbergen, M.W.; Jacques, S.D.M.; Biao, C.; Cernik, R.J.; O'Brien, M.G.; Di Michiel, M.; Weckhuysen, B.M.; Beale, A.M. Noninvasive spatiotemporal profiling of the processes of impregnation and drying within Mo/Al_2O_3 catalyst bodies by a combination of X-ray absorption tomography and diagonal offset Raman spectroscopy. *ACS Catal.* **2013**, *3*, 339–347. [CrossRef]
15. Chakrabarti, A.; Wachs, I.E. Molecular structure–reactivity relationships for olefin metathesis by Al_2O_3-supported surface MoO_x sites. *ACS Catal.* **2018**, *8*, 949–959. [CrossRef]
16. Chen, K.; Xie, S.; Iglesia, E.; Bell, A.T. Structure and Properties of zirconia-supported molybdenum oxide catalysts for oxidative dehydrogenation of propane. *J. Catal.* **2000**, *189*, 421–430. [CrossRef]
17. Christodoulakis, A.; Heracleous, E.; Lemonidou, A.A.; Boghosin, S. An operando Raman study of structure and reactivity of alumina-supported molybdenum oxide catalysts for the oxidative dehydrogenation of ethane. *J. Catal.* **2006**, *242*, 16–25. [CrossRef]

18. Grünert, W.; Stakheev, A.Y.; Feldhaus, R.; Anders, K.; Shpiro, E.S.; Minachev, K.M. Reduction and aromatization activity of MoO_3/Al_2O_3 Catalysts: The identification of the active Mo oxidation state on the basis of reinterpreted Mo 3d XPS spectra. *Studies. Surf. Sci. Catal.* **1993**, *75*, 1053–1064. [CrossRef]
19. Banks, R.L. Olefin metathesis: Technology and applications. In *Applied Industrial Catalysis*; Leach, B.E., Ed.; Academic Press: Orlando, FL, USA, 1984; pp. 215–239.
20. Brandhorst, M.; Cristol, S.; Capron, M.; Dujadin, C.; Vezin, H.; Le bourdon, G.; Payen, E. Catalytic oxidation of methanol on Mo/Al_2O_3 catalyst: An EPR and Raman/infrared operando spectroscopies study. *Catal. Today* **2006**, *113*, 34–39. [CrossRef]
21. Bridgewater, A.J.; Burch, R.; Mitchell, P.C.H. Molybdenum/carbon catalysts for reforming reactions. *J. Chem. Soc. Faraday I* **1980**, *76*, 1811–1820. [CrossRef]
22. Meunier, F.C.; Yasmeen, A.; Ross, J.R.H. Oxidative dehydrogenation of propane over molybdenum-containing catalysts. *Catal. Today* **1997**, *37*, 33–42. [CrossRef]
23. Abello, M.C.; Gomez, M.F.; Ferretti, O. $Mo/\gamma\text{-}Al_2O_3$ catalysts for the oxidative dehydrogenation of propane.: Effect of Mo loading. *Appl. Catal. A* **2001**, *207*, 421–431. [CrossRef]
24. Heracleous, E.; Machli, M.; Lemonidou, A.A.; Vasalos, I.A. Oxidative dehydrogenation of ethane and propane over vanadia and molybdena supported catalysts. *J. Mol. Catal. A Chem.* **2005**, *232*, 29–39. [CrossRef]
25. Abello, M.C.; Gomez, M.F.; Casella, M.; Ferretti, O.A.; Bañares, M.A.; Fierro, J.L.G. Characterization and performance for propane oxidative dehydrogenation of Li-modified MoO_3/Al_2O_3 catalysts. *Appl. Catal. A Gen.* **2003**, *251*, 435–447. [CrossRef]
26. Rostom, S.; de Lasa, H.I. Propane oxidative dehydrogenation using consecutive feed injections and fluidizable $VO_x/\gamma Al_2O_3$ and $VO_x/ZrO_2–\gamma Al_2O_3$ catalysts. *Ind. Eng. Chem. Res.* **2017**, *56*, 13109–13124. [CrossRef]
27. Chen, S.; Zeng, L.; Mu, R.; Xiong, C.; Zhao, Z.-J.; Zhao, C.; Pei, C.; Peng, L.; Luo, J.; Fan, L.-S.; et al. Modulating lattice oxygen in dual-functional Mo–V–O mixed oxides for chemical looping oxidative dehydrogenation. *J. Am. Chem. Soc.* **2019**, *141*, 18653–18657. [CrossRef] [PubMed]
28. Beale, A.M.; van der Eerden, A.M.J.; Kervinen, K.; Newton, M.A.; Weckhuysen, B.M. Adding a third dimension to operando spectroscopy: A combined UV-Vis, Raman and XAFS setup to study heterogeneous catalysts under working conditions. *Chem Commun.* **2005**, 3015–3017. [CrossRef]
29. Brookes, C.; Wells, P.P.; Dimitratos, N.; Jones, W.; Gibson, E.K.; Morgan, D.J.; Cibin, G.; Nicklin, C.; Mora-Fonz, D.; Scanlon, D.O.; et al. The nature of the molybdenum surface in iron molybdate. The active phase in selective methanol oxidation. *J. Phys. Chem. C* **2014**, *118*, 26155–26161. [CrossRef]
30. Chen, K.; Xie, S.; Bell, A.T.; Iglesia, E. Alkali effects on molybdenum oxide catalysts for the oxidative dehydrogenation of propane. *J. Catal.* **2000**, *195*, 244–252. [CrossRef]
31. Brookes, C.; Bowker, M.; Gibson, E.K.; Gianolio, D.; Mohammed, K.M.H.; Parry, S.; Rogers, S.M.; Silverwood, I.P.; Wells, P.P. In situ spectroscopic investigations of MoO_x/Fe_2O_3 catalysts for the selective oxidation of methanol. *Catal. Sci. Technol.* **2016**, *6*, 722–730. [CrossRef]
32. Hu, H.; Wachs, I.E.; Bare, S.R. Surface Structures of supported molybdenum oxide catalysts: Characterization by Raman and Mo L3-edge XANES. *J. Phys. Chem.* **1995**, *99*, 10897–10910. [CrossRef]
33. Payen, E.; Grimblot, J.; Kasztelan, S. Study of Oxidic and Reduced Alumina-Supported Molybdate and Heptamolybdate Species by in Situ Laser Raman Spectroscopy. *J. Phys. Chem.* **1987**, *91*, 6642–6648. [CrossRef]
34. Jawhari, T.; Roid, A.; Casado, J. Raman spectroscopic characterization of some commercially available carbon black materials. *Carbon* **1995**, *33*, 1561–1565. [CrossRef]
35. Coccato, A.; Jehlicka, J.; Moens, L.; Vandenabeele, P. Raman spectroscopy for the investigation of carbon-based black pigments. *J. Raman Spectrosc.* **2015**, *46*, 1003–1015. [CrossRef]
36. Eberly, P.E.; Kimberlin, C.N.; Miller, W.H.; Drushel, H.V. Coke formation on silica-alumina cracking catalysts. *Ind. Eng. Chem. Process. Des. Dev.* **1966**, *5*, 193–198. [CrossRef]
37. Al-Abadleh, H.A.; Grassian, V.H. FT-IR study of water adsorption on aluminum oxide surfaces. *Langmuir* **2003**, *19*, 341–347. [CrossRef]
38. Matam, S.K.; Newton, M.A.; Weidenkaff, A.; Ferri, D. Time resolved operando spectroscopic study of the origin of phosphorus induced chemical aging of model three-way catalysts Pd/Al_2O_3. *Catal. Today* **2013**, *205*, 3–9. [CrossRef]
39. Wijnja, H.; Schulthess, C.P. ATR–FTIR and DRIFT spectroscopy of carbonate species at the aged $\gamma\text{-}Al_2O_3$/water interface. *Spectrochimica Acta Part. A* **1999**, *55*, 861–872. [CrossRef]

40. Davydov, A. *Molecular Spectroscopy of Oxide Catalyst Surfaces*; John Wiley & Sons Ltd.: Chichester, UK, 2003; p. 32.
41. Magg, N.; Immaraporn, B.; Giorgi, J.B.; Schroeder, T.; Baumer, M.; Dobler, J.; Wu, Z.; Kondratenko, E.; Cherian, M.; Baerns, M.; et al. Vibrational spectra of alumina- and silica-supported vanadia revisited: An experimental and theoretical model catalyst study. *J. Catal.* **2004**, *226*, 88–100. [CrossRef]
42. Pazè, C.; Sazak, B.; Zecchina, A.; Dwyer, J. FTIR and UV−vis spectroscopic study of interaction of 1-butene on H−ferrierite zeolite. *J. Phys. Chem. B* **1999**, *103*, 9978–9986. [CrossRef]
43. Lin-Vien, D.; Colthup, N.B.; Fateley, W.G.; Grasselli, J.G. *The Handbook of Infrared and Raman Characteristic Frequencies of Organic Molecules*; Academic Press: Boston, MA, USA, 1991.
44. Rozwadowski, M.; Lezanska, M.; Wloch, J.; Erdmann, K.; Golembiewski, R.; Kornatowski, J. Investigation of coke deposits on Al-MCM-41. *Chem. Mater.* **2001**, *13*, 1609–1616. [CrossRef]
45. Lercher, J.A.; Colombier, C.; Noller, H. Acid–base properties of alumina–magnesia mixed oxides. Part 4.—Infrared study of adsorption of carbon dioxide. *J. Chem. Soc. Faraday Trans. I* **1984**, *80*, 949–959. [CrossRef]
46. Parker, S.F.; Lennon, D.; Albers, P.W. Vibrational spectroscopy with neutrons—A review of new directions. *Appl. Spectrosc.* **2011**, *65*, 1325–1341. [CrossRef]
47. Albers, P.W.; Bösing, S.; Rotgerink, H.L.; Ross, D.K.; Parker, S.F. Inelastic neutron scattering study on the influence of after-treatments on different technical cokes of varying impurity level and sp^2/sp^3 character. *Carbon* **2002**, *40*, 1549–1558. [CrossRef]
48. Albers, P.W.; Weber, W.; Möbus, K.; Wieland, S.D.; Parker, S.F. Neutron scattering study of the terminating protons in the basic structural units of non-graphitising and graphitising carbons. *Carbon* **2016**, *109*, 239–245. [CrossRef]
49. Jackson, S.D.; Grenfell, J.; Matheson, I.M.; Munro, S.; Raval, R.; Webb, G. Deactivation and regeneration of alkane dehydrogenation catalysts. In Proceedings of the 7th International Symposium on Catalyst Deactivation, Cancun, Mexico, 5–8 October 1997; Bartholomew, C.H., Fuentes, G.A., Eds.; Studies in Surface Science and Catalysis. Elsevier: Amsterdam, The Netherlands, 1997; Volume 111, pp. 167–174. [CrossRef]
50. Gibson, E.K.; Beale, A.M.; Catlow, C.R.A.; Chutia, A.; Gianolio, D.; Gould, A.; Kroner, A.; Mohammed, K.M.H.; Perdjon, M.; Rogers, S.M.; et al. Restructuring of AuPd nanoparticles studied by a combined XAFS/DRIFTS approach. *Chem. Mater.* **2015**, *27*, 3714–3720. [CrossRef]
51. Newville, M. *IFEFFIT*: Interactive XAFS analysis and *FEFF* fitting. *J. Synchrotron Rad.* **2001**, *8*, 322–324. [CrossRef]
52. Ravel, B.; Newville, M. *ATHENA*, *ARTEMIS*, *HEPHAESTUS*: Data analysis for X-ray absorption spectroscopy using *IFEFFIT*. *J. Synchrotron Rad.* **2005**, *12*, 537–541. [CrossRef]
53. Gibson, E.; Craswell, J.; Hellier, P.; Catlow, C.R.A.; Parker, S.F.; Matam, S.K. Investigating the Speciation of Hydrocarbonaceous Deposits Formed during Oxidative Dehydrogenation of Propane, STFC ISIS Neutron and Muon Source. 2017. Available online: https://data.isis.stfc.ac.uk/doi/STUDY/103200776/ (accessed on 23 October 2020).
54. Gibson, E.; Craswell, J.; Hellier, P.; Catlow, C.R.A.; Parker, S.F.; Matam, S.K. Investigating the speciation of hydrocarbonaceous deposits formed during oxidative dehydrogenation of propane, STFC ISIS Neutron and Muon Source. 2018. Available online: https://data.isis.stfc.ac.uk/doi/STUDY/103195237/ (accessed on 23 October 2020). [CrossRef]